



HAL
open science

Tandem Hydrogenation/Hydrogenolysis of Furfural to 2-Methylfuran over a Fe/Mg/O Catalyst: Structure–Activity Relationship

Carlo Lucarelli, Danilo Bonincontro, Yu Zhang, Lorenzo Grazia, Marc Renom-Carrasco, Chloé Thieuleux, Elsje Alessandra Quadrelli, Nikolaos Dimitratos, Fabrizio Cavani, Stefania Albonetti

► **To cite this version:**

Carlo Lucarelli, Danilo Bonincontro, Yu Zhang, Lorenzo Grazia, Marc Renom-Carrasco, et al.. Tandem Hydrogenation/Hydrogenolysis of Furfural to 2-Methylfuran over a Fe/Mg/O Catalyst: Structure–Activity Relationship. *Catalysts*, 2019, 9 (11), pp.895. 10.3390/catal9110895. hal-02367895

HAL Id: hal-02367895

<https://hal.science/hal-02367895>

Submitted on 13 Nov 2020

HAL is a multi-disciplinary open access archive for the deposit and dissemination of scientific research documents, whether they are published or not. The documents may come from teaching and research institutions in France or abroad, or from public or private research centers.




L'archive ouverte pluridisciplinaire **HAL**, est destinée au dépôt et à la diffusion de documents scientifiques de niveau recherche, publiés ou non, émanant des établissements d'enseignement et de recherche français ou étrangers, des laboratoires publics ou privés.



Distributed under a Creative Commons Attribution 4.0 International License

Article

Tandem Hydrogenation/Hydrogenolysis of Furfural to 2-Methylfuran over a Fe/Mg/O Catalyst: Structure–Activity Relationship

Carlo Lucarelli ¹, Danilo Bonincontro ², Yu Zhang ^{2,3}, Lorenzo Grazia ²,
Marc Renom-Carrasco ³, Chloé Thieuleux ³, Elsje Alessandra Quadrelli ³,
Nikolaos Dimitratos ², Fabrizio Cavani ² and Stefania Albonetti ^{2,*}

¹ Dipartimento di Scienza e Alta tecnologia, Università dell'Insubria, Via Valleggio 9, 22100 Como, Italy; carlo.lucarelli@uninsubria.it

² Dipartimento di Chimica Industriale “Toso Montanari”, University of Bologna Viale del Risorgimento 4, 40136 Bologna, Italy; danilo.bonincontro2@unibo.it (D.B.); niobium224@gmail.com (Y.Z.); Lorenzo.Grazia@polynt.com (L.G.); nikolaos.dimitratos@unibo.it (N.D.); fabrizio.cavani@unibo.it (F.C.)

³ Université de Lyon, C2P2—UMR 5265 (CNRS—Université de Lyon 1—CPE Lyon), Équipe Chimie; Organométallique de Surface CPE Lyon, 43 Boulevard du 11 Novembre 1918, CEDEX, 69616 Villeurbanne, France; mrenomc@gmail.com (M.R.-C.); thieuleux@cpe.fr (C.T.); quadrelli@cpe.fr (E.A.Q.)

* Correspondence: stefania.albonetti@unibo.it; Tel.: +39-051-2093681

Received: 8 October 2019; Accepted: 23 October 2019; Published: 27 October 2019



Abstract: The hydrodeoxygenation of furfural (FU) was investigated over Fe-containing MgO catalysts, on a continuous gas flow reactor, using methanol as a hydrogen donor. Catalysts were prepared either by coprecipitation or impregnation methods, with different Fe/Mg atomic ratios. The main product was 2-methylfuran (MFU), an important highly added value chemical, up to 92% selectivity. The catalyst design helped our understanding of the impact of acid/base properties and the nature of iron species in terms of catalytic performance. In particular, the addition of iron on the surface of the basic oxide led to (i) the increase of Lewis acid sites, (ii) the increase of the dehydrogenation capacity of the presented catalytic system, and (iii) to the significant enhancement of the FU conversion to MFU. FTIR studies, using methanol as the chosen probe molecule, indicated that, at the low temperature regime, the process follows the typical hydrogen transfer reduction, but at the high temperature regime, methanol dehydrogenation and methanol disproportionation were both presented, whereas iron oxide promoted methanol transfer. FTIR studies were performed using furfural and furfuryl alcohol as probe molecules. These studies indicated that furfuryl alcohol activation is the rate-determining step for methyl furan formation. Our experimental results clearly demonstrate that the nature of iron oxide is critical in the efficient hydrodeoxygenation of furfural to methyl furan and provides insights toward the rational design of catalysts toward C–O bonds' hydrodeoxygenation in the production of fuel components.

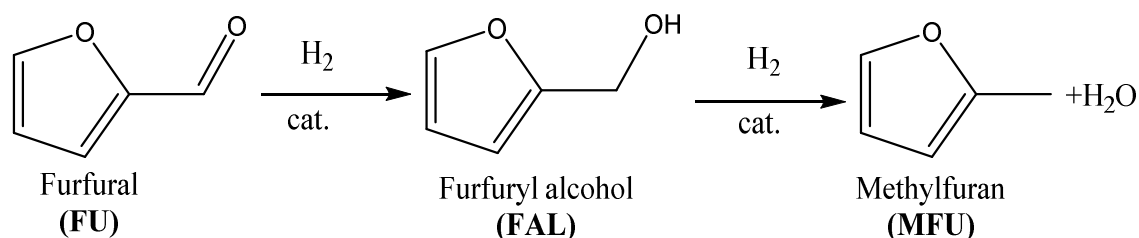
Keywords: furfural; 2 methyl-furan; hydrodeoxygenation; catalyst design; iron; magnesium oxide; catalytic hydrogen transfer reduction; methanol

1. Introduction

The use of biomass, particularly lignocellulosic materials for fuels and chemical production, aims at reducing the exploitation of non-renewable resources. However, the industry is facing the challenge of developing new chemical processes for converting these renewable feedstocks containing highly functionalized carbohydrates into platform molecules with reduced oxygen content [1]. Many of those

systems involve molecular hydrogen as the reductant; at the same time, H-transfer processes, where an organic molecule (e.g., an alcohol) behaves as the hydrogen donor, are a promising alternative [2]. Avoiding the use of H₂ for substrate reduction could induce safer and more selective chemical processes. Indeed, the lower hydrogenating capability of most hydrogen donors promotes a higher degree of control, especially when partially hydrogenated molecules are needed [3]; this is the case in hydrodeoxygenation (HDO) processes, where C–O bonds are selectively cleaved, leaving the nearby C=C and C–C bonds unchanged.

Within bio-derived platform molecules, furan derivatives are important intermediates because of their rich chemistry. For this reason, many efforts were made in the conversion of furfural (FU), which can be large-scale produced from hemi-cellulose into furan-based compounds in the form of furfuryl alcohol (FAL) and 2-methylfuran (MFU) [4]. FAL can be formed by selective hydrogenation of the FU carbonyl group (see Scheme 1). MFU is often produced through further hydrogenolysis of FAL [5–7] and has drawn the attention of researchers as a gasoline alternative due to its very attractive combustion performance in engines [8].



Scheme 1. Sequential reduction of furfural to 2-methylfuran.

Catalytic transfer HDO of furfural was investigated over heterogeneous catalysts using different hydrogen donors in the recent years [9–12]. In our group, the liquid-phase reduction of FU into FAL was carried out using methanol as a hydrogen donor and MgO as a heterogeneous basic catalyst. Furfural was completely reduced into its corresponding alcohol through a Meerwein–Ponndorf–Verley (MPV)-like mechanism [13]. More recently, Hermans and co-workers obtained a 62% yield of 2-methylfuran (and 2-methyltetrahydrofuran) over Pd/Fe₂O₃, using 2-propanol as the H-donor in continuous liquid phase (180 °C, 25 bar) [4]. Vlachos et al. showed that Ru/RuO_x/C catalysts were also active for the liquid-phase transfer hydrogenation of FU to MFU. Thorough mechanistic studies to better understand the reaction mechanism and the role of active sites, supported by DFT calculations, they proposed three different catalytic sites: Lewis acidity in the RuO₂ promotes the transfer hydrogenation of FU to FAL, RuO₂ oxygen vacancies catalyze the C–O scission to form MFU, and metallic Ru helps form hydride species that regenerate the RuO₂ vacancies [14–16].

In the gas-phase furfural hydrogenation reaction, the reaction of furfural with hydrogen over an SiO₂-supported transition metal catalyst was investigated by D.E. Resasco [17]. They specified that η¹ (O) aldehyde is the mostly likely species adsorbed on the Cu surface, which will favor furfuryl alcohol formation. Furthermore, they indicated that surface η² (C=O) adsorption geometry facilitated the formation of methyl furan [18,19]. Other groups have shown that Fe promotes methyl furan formation in Ni–Fe systems [20] and Fe–Cu systems [6,21]. The authors concluded that the addition of Fe suppresses the decarbonization and promotes the C=O hydrogenation at low temperatures and the C–O hydrogenolysis at high temperatures. Moreover, it reveals that the partial reduction of Fe³⁺ to Fe²⁺ played the role of promoter. However, it is still unclear what the exact role of Fe in the hydrogen-transfer processes is.

Recently, we observed high MFU yield (79%) in the gas-phase reduction of furfural, using methanol as the hydrogen donor over an iron–magnesium mixed oxide catalyst (Fe/Mg/O) [22]. In that work, we showed that the introduction of Fe³⁺ cations into the magnesia structure leads to the formation of higher quantities of MFU, derived from FAL hydrogenolysis, without presenting a detailed structure–activity correlation study. Since iron is known to have both redox and acid–base properties [23], we focused

on studying the role of Fe in the Fe/MgO catalytic system, in order to determine structure–activity relationships. Therefore, in the current study, catalysts with different iron content were prepared, in order to investigate this relationship in MFU formation. Fe/Mg/O catalysts were synthesized either by coprecipitation or incipient wetness impregnation methods, to understand how the preparation routes affect the activity and product distribution of FU transformation. The synthesized materials were thoroughly characterized and compared based on their redox and acid–base properties and their crystalline phase. Finally, we carried out in situ DRIFT studies to elucidate (i) the activity and selectivity determining factors, (ii) the influence of the basicity, and (iii) the nature of FeO_x species for the hydrogenation/hydrogenolysis of furfural with the purpose of exploring the role of FeO_x/MgO in terms of furfural activation and production of MFU.

2. Results and Discussion

2.1. Physical–Chemical Properties of the Iron-Containing MgO Catalyst

Several Fe/Mg/O catalysts containing different Fe/Mg atomic ratios were prepared both by coprecipitation and by incipient wetness impregnation methods, as described in the experimental section. Characterizations of these materials are summarized in Table 1.

Table 1. Physicochemical properties (specific surface area, crystalline phase, Lewis acidity, Brønsted acidity and basicity) of MgO, Fe₂O₃ and Fe/Mg/O coprecipitated and synthesized by incipient wetness impregnation samples.

Catalyst	Fe:Mg	Surface Area (m ² ·g ⁻¹)	Crystalline Phase (XRD)	Lewis Acidity (mmol·g ⁻¹) ^(a)	Brønsted Acidity (mmol·g ⁻¹) ^(a)	Basicity (mmol·g ⁻¹) ^(b)
MgO		172	Periclase MgO	0	0	7.51
Fe ₂ O ₃		51	Hematite	- ^(d)	- ^(d)	1.38
Fe/Mg/O_1_10	1:10	102	Periclase MgO	0	0	2.62
Fe/Mg/O_1_2	1:2	140	Periclase MgO and Magnetite/Magnesioferrite	0.43 [0.20 + 0.07 + 0.16] ^(c)	0	2.34
Fe/Mg/O_1_1	1:1	74	Periclase MgO and Magnetite/Magnesioferrite	0.62 [0.25 + 0.24 + 0.13] ^(c)	0	1.09
FeOx/MgO_1_100	1:100	150	Periclase MgO	0	0	2.62
FeOx/MgO_1_20	1:20	129	Periclase MgO and Hematite	0	0	2.34
FeOx/MgO_1_10	1:10	94	Periclase MgO and Hematite	0.15 [0.05 + 0.06 + 0.04] ^(c)	0	2.67
FeOx/MgO_1_2	1:2	33	Periclase MgO and Hematite	0.29 [0.04 + 0.17 + 0.08] ^(c)	0	0.96

^(a) Quantification of surface Lewis and Brønsted acid sites was obtained from Pyridine-FTIR analysis. ^(b) Basicity measurements were performed by TPD analysis using CO₂ as probe molecule. ^(c) Distribution of the Lewis acid sites among weak, medium, and strong sites, respectively, based on the temperature at which pyridine desorption is observed, i.e., 20–200 °C (weak), 200–400 °C (medium), and >400 °C (strong). ^(d) Not possible to analyze by this technique.

The addition of Fe generally caused the decrease of surface area both in the case of coprecipitated and impregnated samples. In the case of impregnation, the decrease of surface area is more pronounced because, in this case, the total amount of iron oxides is located on the surface of MgO; in the case of the coprecipitated samples, the amount of superficial Fe may be less significant (Table 1). This assumption may be supported by the XRD analysis, which revealed that, in the case of the impregnated samples, the iron-containing phases are detected, even at a low concentration (i.e., from 20:1 Mg:Fe molar ratio on, Figure 1).

In the case of coprecipitated samples (Figure 1a), the main crystalline phase detected is ascribed to the MgO-periclase phase. There is no indication on the Fe intercalation in the MgO lattice, but a new

crystalline phase arises by increasing the Fe content, and such a phase could be ascribed to Magnetite or Magnesioferrite; among the two, the latter is more likely formed since periclase diffraction peak intensities decrease, because the incorporation of trivalent Fe^{3+} cation in the periclase lattice is known to generate cationic defects and to produce a low crystalline degree [24–26]. Conversely, the samples prepared by impregnation (Figure 1b) show periclase as the main phase, with no evidences of mixed Mg/Fe phases, since only the Hematite crystalline phase was detected alongside the one of periclase. This confirms that addition of Fe by impregnation on the MgO does not influence periclase crystallinity.

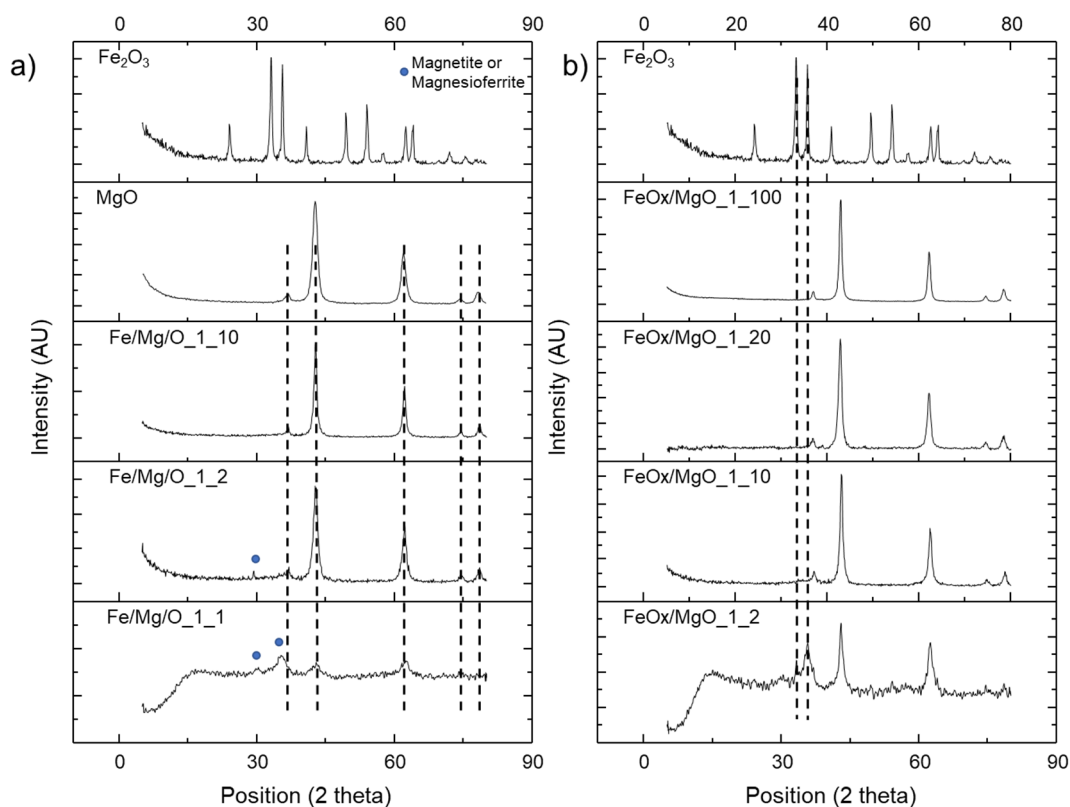


Figure 1. XRD patterns of (a) coprecipitated samples and (b) impregnated samples.

Fe addition is expected to introduce both acid and redox properties in the mixed oxide [23]. FTIR studies were carried out using pyridine as the chosen probe molecule. The pyridine adsorption-desorption FTIR (Py-FTIR) spectra were recorded and reported in Figures S1 and S2 for the coprecipitated samples, and in Figures S3 and S4 for the impregnated ones; the relative acidity measurements are summarized in Table 1. In all cases, the absence of band at 1540 cm^{-1} , which is the characteristic band of Brønsted acid sites, and the presence of a band at 1444 cm^{-1} , corresponding to the adsorption of Pyridine at the Lewis acid sites, showed that only Lewis acid sites were present in Fe/Mg/O that showed acidity. The specific amounts of weak, medium, and strong basic sites are reported in Table 1. The weak sites are defined as the ones from which pyridine is removed by evacuation at 200 °C ; the medium weak sites correspond to pyridine evacuation between 200 and 400 °C ; and, finally, the strong sites correspond to pyridine evacuation above 400 °C [27]. Semi-quantitative evaluation of the surface acid sites was obtained by peak integration. The integration of the bands allowed for a few comparisons to be made to determine the effect of the Fe content and the effect of the synthesis method. The increase of the Fe amount led to an increase in total acidity and change in the distribution among different-strength acid sites. In the case of the impregnation method, the pyridine was adsorbed on the samples with Fe/Mg 1/10 molar ratio; in the case of the coprecipitation method, the adsorption of the probe molecule occurred only on the samples with an Fe/Mg of 1/1 and 1/2 molar ratio. Moreover, samples with the same Fe/Mg molar ratio, but prepared with different experimental methods, showed

different characteristics; in particular, the coprecipitated ones displayed higher total acidity than the ones obtained by impregnation.

TPD analysis, using CO_2 as the probe molecule, was performed to determine basic properties of the samples. The results are presented in Table 1 and Figure 2. Based on the desorption temperature of CO_2 , the adsorption is usually classified into three categories: weak adsorption ($25\text{--}125\text{ }^\circ\text{C}$), medium adsorption ($125\text{--}225\text{ }^\circ\text{C}$), and strong adsorption ($>225\text{ }^\circ\text{C}$), which are assigned to surface hydroxyl groups, oxygen in $\text{Mg}^{2+}\text{-O}^{2-}$ pairs, and low coordination oxygen anions, respectively [28].

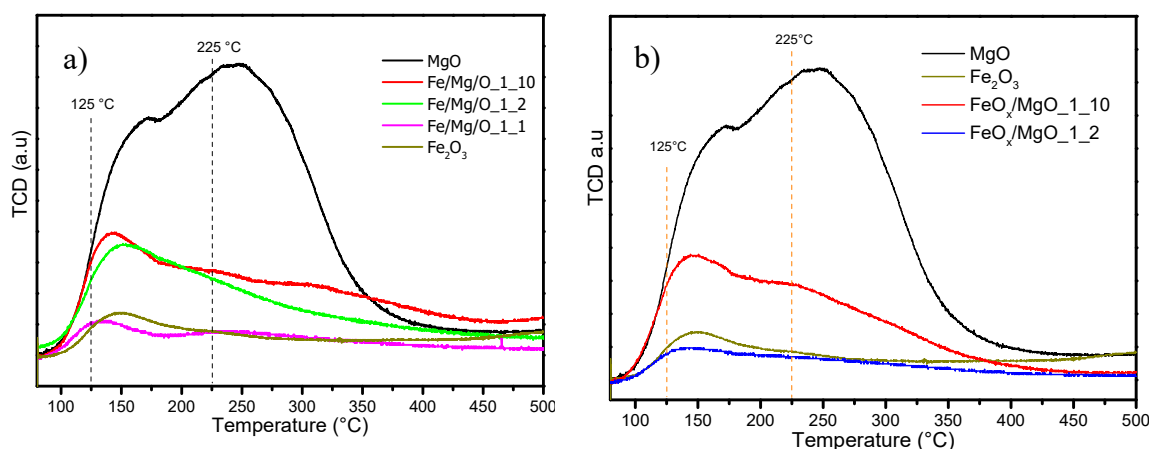


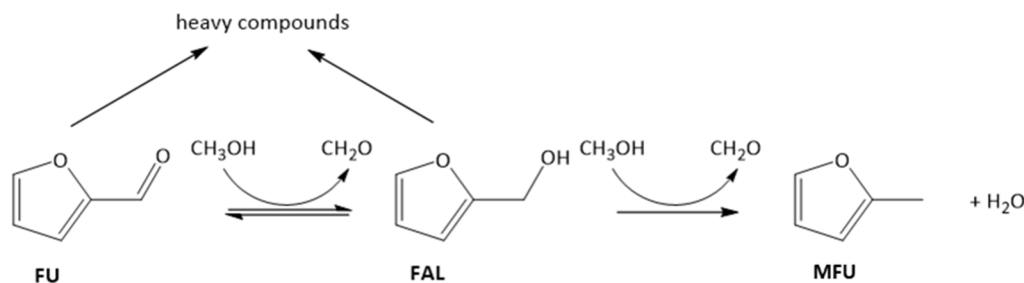
Figure 2. CO_2 -TPD curves of: (a) coprecipitated Fe/Mg/O samples, MgO, and Fe_2O_3 ; and (b) impregnated FeO_x/MgO samples, MgO, and Fe_2O_3 .

Catalysts with a higher Fe/Mg molar ratio showed lower basicity values because of the higher electronegativity of Fe^{3+} species, with respect to Mg^{2+} species. As a consequence, the charge density decreases and makes the O^{2-} less electrophilic than in pure MgO [29].

The higher basicity of the Fe/Mg 1/2 molar ratio coprecipitated sample with respect to the analogous impregnated one may be attributed to the different crystalline phases formed at such a high Fe concentration.

2.2. Reactivity Tests of Iron/Magnesium Oxide Catalysts in the Hydrodeoxygenation of Furfural

In our previous work, FU was converted to MFU, with methanol as the hydrogen source, through a tandem hydrogenation/hydrogenolysis sequence, using MgO and Mg/Fe/O_1_2 catalysts (Scheme 2) [22].



Scheme 2. Reaction pathways for furfural hydrodeoxygenation.

The catalytic systems in the reported operative conditions (optimized in a previous work [22]) were both active in FU conversion; however, their different chemical–physical properties led to different product selectivity. MgO was selective to FAL, while the mixed oxide produced preferentially MFU. We report hereafter a detailed study aiming at explaining the role of Fe in this change of selectivity.

The catalytic performances of the coprecipitated Fe/Mg/O catalysts described in Table 1 for furfuryl alcohol (FAL) and methyl furan (MFU) production from furfural (FU) are reported in Figure 3.

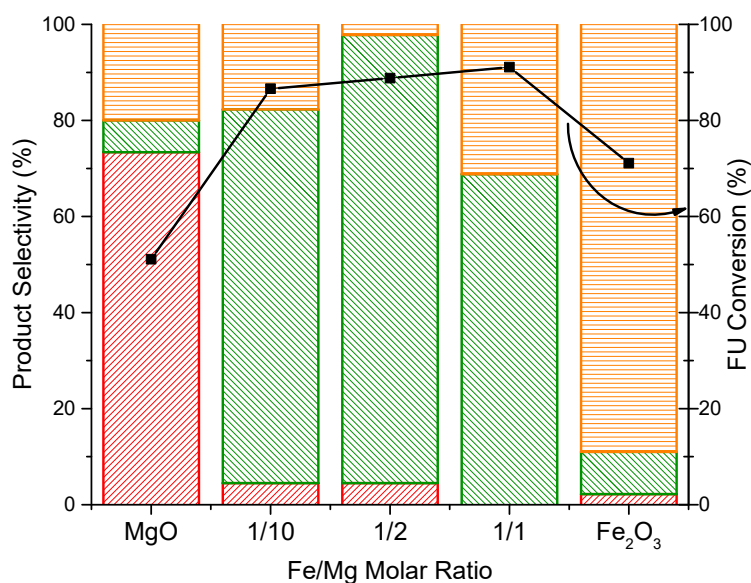






Figure 3. Profiles of coprecipitated Fe/Mg/O mixed oxide catalysts with different Fe content levels. Feed composition: 5% FU, 50% CH₃OH, 45% N₂, 1 atm, overall gas contact time 1.1 s, reaction time 1 h, 380 °C. Legend: FAL  MFU  Carbon loss  FU conversion .

In the reaction with MgO, the H-transfer hydrogenation occurred with a high selectivity and moderate conversion toward FAL. However, under these experimental conditions, MgO exhibited limited activity in the further hydrogenolysis to MFU. The formation of some side products, consistent with the C-loss (20%), was also observed. Compared with pure MgO, the presence of Fe improved furfural conversion and methyl furan selectivity. Notably, when a low amount of iron (Fe/Mg = 1/10) was introduced, the selectivity of MFU was significantly increased from 5% to 80%, while furfural conversion increased from 52% to 88%. The maximum MFU selectivity (92%) was achieved when using Fe/Mg/O with Fe/Mg = 1/2 molar ratio. A further increase of the Fe content (Fe/Mg molar ratio 1/1) significantly decreased the MFU formation (70% selectivity) and led to a poor carbon balance, probably due to higher heavy compounds' deposition on the catalyst surface [22].

Therefore, Fe introduction favored the formation of the targeted MFU. FAL hydrogenolysis to form MFU was strongly influenced by the amount of Fe introduced in the catalyst and by the changes in its chemical–physical properties.

When the basicity density decreased from MgO (7.51 mmol/g) to Fe/Mg/O_1_2 (2.34 mmol/g), a clear enhancement in MFU yield was observed, indicating that MFU formation was not related to the presence of basic sites. Although the good selectivity showed by Fe/Mg/O_1_2 could be also ascribed to the presence of acidic sites, an excess in acidity will be detrimental for the selectivity toward MFU. Indeed, as suggested by the high conversion but poor selectivity obtained with pure iron oxide, a high level of acidity could promote side reactions (from FU and/or FAL).

Further catalytic tests in the same experimental reaction conditions were carried out using the impregnated samples (Figure 4). For this series of catalysts, the formation of MFU was enhanced by the addition of Fe; high selectivities (74%–88%) were observed with Fe/Mg molar ratios in the range of 1/20 to 1/2.

The catalytic results obtained with the two series of Fe/Mg/O samples show that the best performances were obtained with the Fe/Mg ratio of 1/2 and of 1/10, for the coprecipitated and impregnated samples, respectively. This suggests that the key parameter for the high selectivity to MFU is the interaction between Fe and the MgO surface. Indeed, in the coprecipitated samples, the Fe

is likely present as Magnesioferrite, while, in the impregnated one, Fe_2O_3 does not change its phase in coexistence with the magnesium-based periclase phase.

In order to better understand the role of acid–base properties of these samples, the effect of acidity and basicity was studied in samples prepared by replacing (i) Fe with Al or (ii) MgO with SiO_2 , respectively.

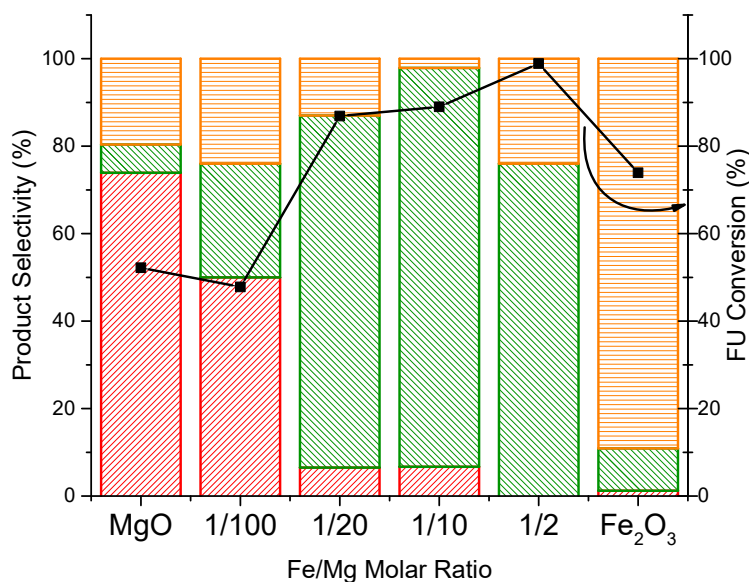






Figure 4. Reaction profiles of impregnated FeO_x/MgO mixed oxide catalysts with different Fe content levels. Feed composition: 5% FU, 50% CH_3OH , 45% N_2 , 1 atm, overall gas contact time 1.1 s, reaction time 1 h, 380 °C. Legend: FAL  MFU  Carbon loss  FU conversion .

2.3. Effect of the Properties of the Synthesized Catalysts on the Product Distribution of FU Reaction

In the literature, the hydrodeoxygenation capacity of a catalyst is generally associated with the presence of Lewis acid sites in the catalytic system; typical examples are niobium oxide [30] and zeolites [31], which were used in liquid phase. Indeed, it was reported that the acid functionalities catalyze the dehydration of alcohol to form intermediates, which will be substituted by surface hydrides. On metal oxides, it was reported that the electron-rich oxygen anions show basic properties and electron-donating character, while the electron-deficient metal cations show acidic character. Basic and hydrogen-abstracting properties of MgO can be modulated with the introduction of host cations, typically trivalent metal cations. While $\text{Fe}/\text{Mg}/\text{O}$ catalysts exhibited both Lewis acid properties and a moderate to strong redox capacity, the $\text{Al}/\text{Mg}/\text{O}$ system has no redox capacity [23]. In order to verify the contribution of the Lewis acid properties on the reaction network, Al^{3+} was chosen as a dopant metal to modify MgO. Indeed, Al^{3+} was reported to be a typical Lewis acid [32]. Therefore, in order to investigate the reaction pathways and product distribution influenced by Lewis acid properties, the catalytic behavior of the best catalysts for the two series (coprecipitated $\text{Fe}/\text{Mg}/\text{O}_{1_2}$ and impregnated $\text{FeO}_x/\text{MgO}_{1_10}$) were compared by substituting Fe with Al, leading to coprecipitated $\text{Al}/\text{Mg}/\text{O}_{1_2}$ and impregnated $\text{Al}_2\text{O}_3/\text{MgO}_{1_10}$. Such synthesized catalysts were studied using the same experimental conditions as for $\text{Fe}/\text{Mg}/\text{O}$. The main properties of Al-containing MgO samples are summarized in Table 2. It is worth noting that the big difference in surface area, between the impregnated and the coprecipitated samples, is due to the specific method of synthesis and composition. Both samples present only the periclase phase for MgO.

The acidity and basicity for these samples were analyzed, and the results are presented in Table 2. Al-containing samples showed a higher degree of acidity compared to the corresponding $\text{Fe}/\text{Mg}/\text{O}$ samples, independently of the choice of the preparation method (see Table 1).

Table 2. Physicochemical properties (specific surface area, crystalline phase, Lewis acidity, Brønsted acidity and basicity) of different Al-containing MgO samples.

Catalyst	Surface Area (m ² ·g ⁻¹)	Crystalline Phase (XRD)	Lewis Acidity (mmol·g ⁻¹) ^(a)	Brønsted Acidity (mmol·g ⁻¹) ^(a)	Basicity (mmol·g ⁻¹) ^(b)
Al/Mg/O_1_2	132	Periclase MgO	0.80 [0.59 + 0.03 + 0.17] ^(c)	0	4.48
AlO _x /MgO_1_10	28	Periclase MgO	0.59 [0.40 + 0.13 + 0.06] ^(c)	0	2.54

^(a) Quantification of Lewis and Brønsted acid sites was obtained from Pyridine-FTIR analysis. ^(b) Basicity measurements were performed by TPD analysis, using CO₂ as a probe molecule. ^(c) Distribution of the Lewis acid sites among weak, medium, and strong sites, respectively, based on the temperature at which pyridine desorption is observed; i.e., 20–200 °C (weak), 200–400 °C (medium), and >400 °C (strong).

Catalytic results are summarized in Table 3, where Al-based materials are compared to the analogous MgO and Fe-containing catalysts. Al/Mg/O_1_2 reached a conversion of 63% with a 37% of carbon loss and an MFU selectivity of 22%. The comparison between Al/Mg/O_1_2 and Fe/Mg/O_1_2 indicated that the former catalyst converted less FU and showed a greater carbon loss, probably due to the increased acidity. Indeed, Py-FTIR analysis (Tables 1 and 2) showed that the total amount of acid sites in Al/Mg/O_1_2 was twice as much as the one of Fe/Mg/O_1_2. This seems to indicate that the presence of Lewis acid sites is not the only feature leading to MFU formation. Moreover, the high acidity clearly increased by-product formation, as demonstrated by the higher carbon loss observed (37%).

Table 3. Summary of the catalytic performance over different Al, Fe doping MgO catalysts.

Catalyst	M/Mg Molar Ratio	FU Conv (%)	FAL Sel (%)	MFU Sel. (%)	C-Loss (%)
MgO	-	52	75	5	20
Al/Mg/O_1_2	1:2	63	41	22	37
Fe/Mg/O_1_2	1:2	93	5	92	3
AlO _x /MgO_1_10	1:10	40	76	5	19
FeO _x /MgO_1_10	1:10	89	5	88	7

Feed composition: 5% FU, 50% CH₃OH, 45% N₂, 1 atm, overall gas contact time 1.1 s, reaction time 1 h, 380 °C.

The same catalytic trend was observed for the impregnated catalysts. AlO_x/MgO_1_10 showed a catalytic performance similar to that of MgO. Comparison with FeO_x/MgO_1_10 was not relevant, since a very low amount of MFU was formed.

In order to illustrate the importance of basicity and its contribution in the reaction system, we prepared a catalyst containing iron oxide as the main component, but with a support that did not present any basicity, i.e., SiO₂, with a Fe/Si atomic ratio equal to 1/10.

The FeO_x/SiO₂_1_10 catalyst showed low furfural conversion (19%), which led principally to decomposition products and low selectivity to MFU (25%) (Table 4). In comparison with Fe₂O₃, a similar product distribution was observed, but with a lower furfural conversion, due to the dilution of FeO_x with SiO₂.

All these experiments led us to conclude that (i) FAL formation is related to surface basicity, (ii) Lewis acidity favors MFU formation—although it does not seem to be the key factor—(iii) the presence of Fe is crucial for MFU production, and (iv) an excess of acidity can enhance the formation of degradation products. For these reasons, it is evident that the precise choice of Fe/Mg molar ratio is crucial to obtain a high MFU selectivity. It is also important to notice that MFU is the main product in FeO_x-based catalysts, even at very low FU conversion; in other words, the almost exclusive formation of MFU is not due to the higher reactant conversion—which would imply the transformation of the intermediately formed FAL—but is strictly related to catalysts' surface properties.

Table 4. Summary of the catalytic performances of silica-supported iron oxide and comparison with bulk Fe₂O₃ and MgO.

Entry	Catalyst	Fe/Si Molar Ratio	FU Conv (%)	FAL Sel (%)	MFU Sel. (%)	C-Loss (%)
1	MgO	-	52	75	5	20
2	Fe ₂ O ₃	-	73	2	10	88
3	SiO ₂	-	0	0	0	0
4	FeO _x /SiO ₂ _1_10	1:10	19	1	25	74

Feed composition: 5% FU, 50% CH₃OH, 45% N₂, 1 atm, overall gas contact time 1.1 s, and reaction time 1 h, 380 °C.

2.4. Mechanistic Insights

In the previous section, it was shown that variations in Fe content for Fe/Mg/O catalysts led to very different product distributions. The key factor influencing the methyl furan selectivity was demonstrated to be the presence of FeO_x species. This section aims to provide some mechanistic insights to explain the observed selectivity trend through in situ DRIFT studies. When dealing with hydrogen transfer processes, two main cycles should be considered: (i) the activation of the hydrogen donor—methanol, in this study—and (ii) the activation of the substrate, furfural or furfuryl alcohol. In order to understand the reaction pathways, the three main components of reaction (methanol, furfural and furfuryl alcohol) were investigated separately on three different model catalytic surfaces, with different properties, as we explained in the previous sections, and based on our current catalytic observations. MgO, Fe₂O₃, and the mixed oxide obtained by the impregnation method, FeO_x/MgO_1_10. The IR spectra of the different catalysts were acquired at different temperatures in the range from 25 to 400 °C.

2.4.1. Methanol Adsorption

The spectra of methanol adsorbed on bulk MgO, bulk Fe₂O₃, and FeO_x/MgO 1/10, after outgassing at different temperatures, are shown in Figure 5a–c, respectively.

When methanol was adsorbed on MgO, at room temperature, two sets of peaks could be observed in the C–H region: one at 2942 and 2835 cm⁻¹, corresponding to physisorbed methanol, and the other at 2917 and 2800 cm⁻¹, assigned to mono-coordinated methoxy groups [33]. The ν_s(C=O) bands corresponding to those species could be found at 1058 and 1108 cm⁻¹, respectively [34]. When the temperature was increased from room temperature to 150 °C, new peaks appeared at 2809 and 1092 cm⁻¹, which were attributed to bridged methoxy species. Further increase of the temperature caused a rapid formation of a species, which could be attributed to a formate isomer, since it displayed a ν_s(CH) peak at 2846 cm⁻¹, a characteristic ν_{as}(COO) at 1600–1610 cm⁻¹, and the ν_s(COO) peaks in the 1379–1339 cm⁻¹ region [35,36].

At 300 °C, only formate and bridged methoxy species could be observed, and at 380 °C (the reaction temperature), only formate was present on the MgO surface.

Exposure of α-Fe₂O₃ to methanol stream at room temperature gave rise to different IR absorption bands: similarly to what was observed in the case of MgO surface, the peaks at 2942, 2832 cm⁻¹ were due to physical adsorbed methanol, and the ones at 2902, 2802, and 1071 cm⁻¹ corresponded to the presence of methoxy species. At 300 °C, the methoxy bands completely disappeared and a substantial amount of formate was formed. This formate was activated in two different modes, with ν_s(CH) peaks at 2853 and 2804 cm⁻¹, ν_{as}(COO) at 1644 and 1611 cm⁻¹, and the ν_s(COO) around 1300 cm⁻¹. Outgassing at 380 °C caused the disappearance of the formate species (no CH vibrations observed), giving way to the presence of new species, presumably carbonates, suggested by the absence of C–H stretching bands at around 2800 cm⁻¹ while still observing ν_s and ν_{as}(COO) bands.

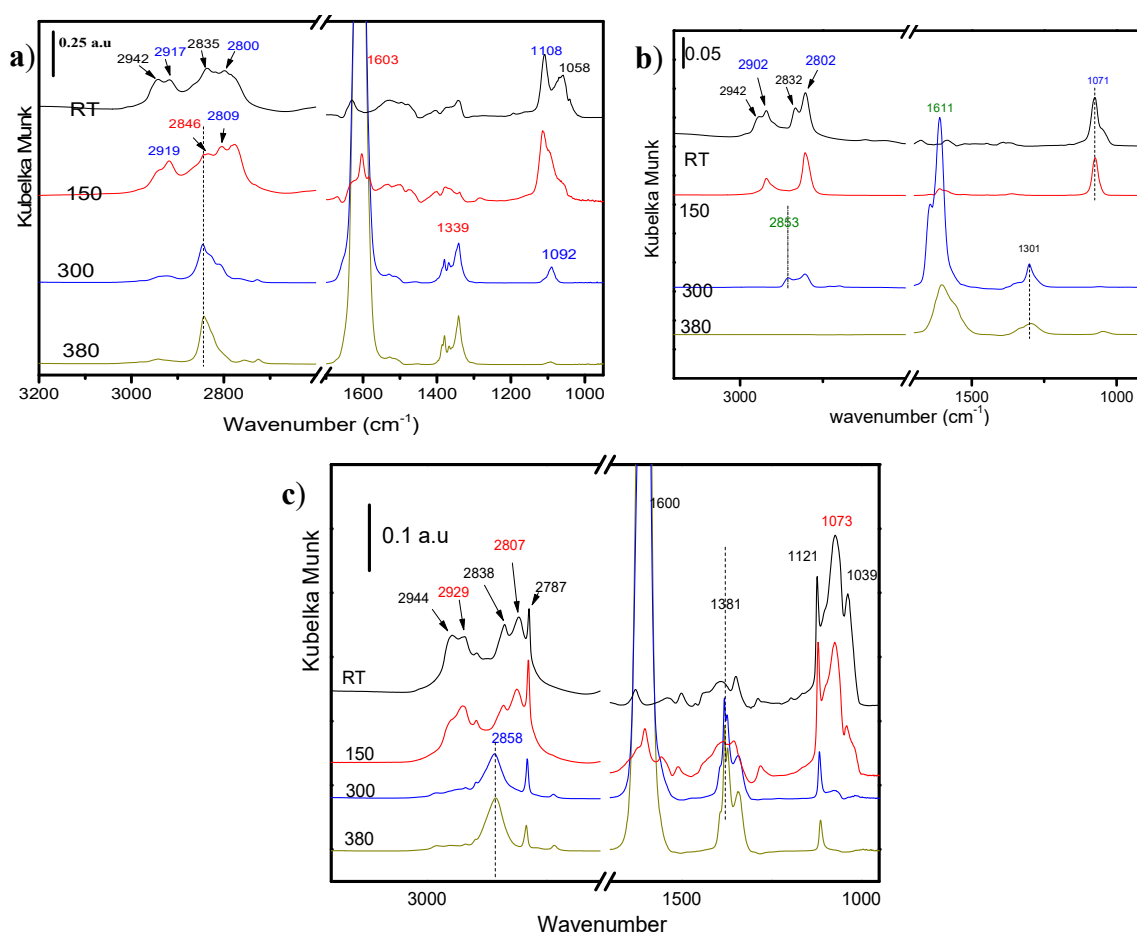


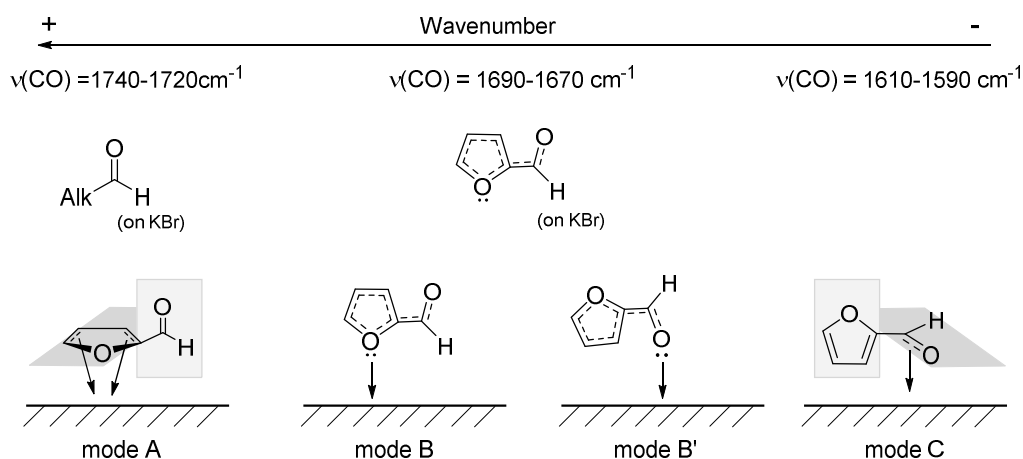
Figure 5. Methanol desorption spectra on (a) MgO, (b) Fe₂O₃, and (c) impregnated FeO_x/MgO_1_10 samples.

Similar to what was observed with the other two surfaces, at room temperature, only physisorbed methanol and methoxy species were present on the surface of the FeO_x/MgO_1_10 sample (C–H vibrations between 2944 and 2807 cm^{−1}, and C–O stretching at 1073 and 1039 cm^{−1}). When increasing the temperature, physisorbed methanol rapidly dissociated to give methoxy species, which, at 300 °C was already completely converted into formate (peaks 1600 and between 1385 and 1330 cm^{−1}).

From these series of experiments, it is possible to conclude that methanol adsorbs in a similar way on the three oxides, with the only differences being the presence of two modes of adsorption of the methoxy species in case of pure MgO.

2.4.2. Furfural and Furfuryl Alcohol Adsorption

Understanding the adsorption geometry of furfural and furfuryl alcohol on the catalytic surface is useful for the comprehension of the reaction network. From the current literature [17,20,37–45], it is possible to propose different coordination modes of the furfural with the surface: either through its aldehyde group or through the furan ring, as shown in Scheme 3.



Scheme 3. Proposed rationalization of the literature observed $\nu(\text{CO})$ in free furfural and physisorbed furfural, depending on the possible coordination modes.

When furfural was adsorbed on MgO, at room temperature (Figure S5), three peaks arising from the C=O stretching could be observed: at 1720, 1672, and 1600 cm^{-1} , corresponding to the modes A, B, and C (Scheme 3, respectively). The peak at 1569 cm^{-1} arises from the C=C of the furan ring. As the temperature increased, the peaks at 1720 and 1672 cm^{-1} decreased, and at 380 °C only the $\eta^2(\text{C}=\text{O})$ mode of activation was present (peak at 1600 cm^{-1}). This suggests that, at this temperature, we have an optimum activation of the C=O bond, which might favor the formation of the furfuryl alcohol [18,46,47]. Furthermore, this experiment demonstrates that adsorbed furfural on MgO is stable even at high temperatures, as was already confirmed by Albonetti et al. [22].

The FTIR adsorption of furfural over Fe_2O_3 could not be performed due to the opacity of the obtained pellets; thus, the experiment was directly carried out with $\text{FeO}_x/\text{MgO}_{1_10}$ (see Figure S6). The obtained spectra were very similar to those of MgO, with the only exception that no peak at 1720 cm^{-1} (corresponding to the furan ring adsorption on the surface) was observed. This may suggest that the presence of FeO_x on the MgO causes a stronger interaction furfural-surface at lower temperatures.

At room temperature, the spectrum of adsorbed furfuryl alcohol over MgO was very similar with respect to the spectrum taken over KBr, meaning that very weak interactions were taking place. When the temperature increased, the furfuryl alcohol bands slowly decreased giving place to the appearance of a band at 1587 cm^{-1} , which, at 400 °C, overlapped with a band at 1602 cm^{-1} . This latter band is the same that was observed for the adsorption of furfural on MgO (see Figure S7). This result proves that, although high temperatures are required, furfuryl alcohol can be dehydrogenated on the MgO surface. Furthermore, it also shows the stability of these two compounds on MgO. A very similar spectrum was obtained when adsorbing furfuryl alcohol at room temperature on $\text{FeO}_x/\text{MgO}_{1_10}$. (Figure S8). However, the dehydrogenation of the alcohol was initiated at lower temperatures (starting at 300 °C) than in the case of MgO. At 380 °C, the band corresponding to furfuryl alcohol almost disappeared and was converted into furfural, as it can be followed by the band at 1505 cm^{-1} .

This section may be divided by subheadings. It should provide a concise and precise description of the experimental results, their interpretation, and the experimental conclusions that can be drawn.

3. Materials and Methods

3.1. Catalyst Preparation

Coprecipitated samples—The MgO and Fe/Mg/O mixed oxide catalysts were prepared, via the precipitation method, from an aqueous solution containing the corresponding metal nitrates $\text{Mg}(\text{NO}_3)_2 \cdot 6\text{H}_2\text{O}$ and $\text{Fe}(\text{NO}_3)_3 \cdot 9\text{H}_2\text{O}$ (Sigma-Aldrich, St. Louis, MO, USA) in different atomic ratios (procedure described in our previous work [24]). All samples were then dried at 120 °C for 2 h and

then calcined in static air at 450 °C for 5 h. Samples were labeled as Fe/Mg/O_n_m, where n_m refers to the Fe-to-Mg molar ratio. The Al/Mg/O sample was prepared via the same experimental procedure, using $\text{Al}(\text{NO}_3)_3 \cdot 9\text{H}_2\text{O}$ (Sigma-Aldrich, St. Louis, MO, USA) as the precursor and named similarly. Bulk Fe_2O_3 and MgO were synthesized by precipitation of the corresponding nitrates.

Impregnated samples— FeO_x supported over MgO samples were prepared by incipient wet impregnation, using $\text{Fe}(\text{NO}_3)_3 \cdot 9\text{H}_2\text{O}$. The amount of nitrate required to obtain samples with a nominal Fe/Mg molar range of 1:100 to 1:10. All samples were then dried at 120 °C for 2 h and then calcined in static air at 450 °C for 5 h. Samples were labeled as $\text{FeO}_x/\text{MgO}_n_m$, where n_m refers to the Fe to Mg molar ratio. AlO_x/MgO and $\text{FeO}_x/\text{SiO}_2$ samples were prepared via the same experimental procedure, using $\text{Al}(\text{NO}_3)_3 \cdot 9\text{H}_2\text{O}$ or silica (W. R. Grace & Co.-Conn., Columbia, MD, USA) as support, and named accordingly.

3.2. Characterization of Catalysts

The BET specific surface area of each catalyst was determined by N_2 absorption–desorption at liquid N_2 temperature, using a Sorptly 1750 Fison instrument (Milan, Italy). Then, 0.3 g of the sample was typically used for the measurement; the sample was outgassed at 150 °C before N_2 absorption.

X-ray diffraction analyses (XRD) of the catalysts were recorded with Ni-filtered $\text{Cu K}\alpha$ radiation ($\lambda = 1.54178 \text{ \AA}$) on a Philips X'Pert vertical diffractometer equipped with a pulse height analyzer and a secondary curved graphite–crystal monochromator.

Chemisorption experiments were carried out on a BELSORB-max from BEL JAPAN. Typically, 100 mg of catalyst was degassed at 450 °C for 3 h under a $50 \text{ mL}\cdot\text{min}^{-1}$ flow of pure helium. After cooling to 80 °C, CO_2 was adsorbed by flowing the catalysts under 50% CO_2 -He gas mixture for 30 min ($50 \text{ mL}\cdot\text{min}^{-1}$), followed by He treatment at 80 °C for 15 min, to remove physisorbed molecules. The catalysts were then heated under He flow ($50 \text{ mL}\cdot\text{min}^{-1}$), up to 500 °C, at a heating rate of $10 \text{ }^\circ\text{C}\cdot\text{min}^{-1}$.

FTIR measurements were carried out in Perkin Elmer Spectrum spectrophotometer (Waltham, MA, USA), between 4000 and 400 cm^{-1} . Self-supported wafers of the samples containing around 35 mg (13 mm diameter) were evacuated at 10^{-5} mbar and 450 °C for 1 h. After cooling to room temperature, the spectrum was recorded and used as background for all subsequent spectra. The sample wafer was then exposed to pyridine vapors at room temperature for 30 min, until equilibrium was reached, and a second spectrum was recorded. Then, the wafer was subjected to evacuation for 10 min, and the spectrum was recorded and labeled as RT. Subsequent evacuations were performed at 100, 200, 300, and 400 °C for 10 min, followed by spectral acquisitions at room temperature [37,48–50].

3.3. Catalytic Tests

Catalytic tests were carried out in a continuous-flow fixed-bed micro-reactor (Pyrex, length 38 cm, internal diameter 1/3 inch), already used for the FU reduction [22,51]. The catalyst (30–60 mesh particles) was placed in the reactor in order to have the contact time equal to 1.1 s, and then it was heated to 380 °C under N_2 flow ($26 \text{ mL}\cdot\text{min}^{-1}$). The catalytic reaction was initiated by the vaporization of methanol and furfural (Sigma-Aldrich, St. Louis, MO, USA) in a 10/1 molar ratio, using the N_2 flow as the carrier gas ($26 \text{ mL}\cdot\text{min}^{-1}$). Furfural was purified via distillation prior to being fed into the flowing gas stream. The total volumetric flow rate through the catalytic bed was held constant at $60 \text{ mL}\cdot\text{min}^{-1}$, and the concentration of furfural, methanol, and nitrogen were respectively 5%, 50%, and 45%. An analysis of reactants and products was carried out as follows: the outlet stream was scrubbed for 1 h, using a cold-trap glass tube (acetonitrile solution, which was maintained at $-26 \text{ }^\circ\text{C}$ by a F32 Julabo Thermostat, Seelbach, Baden-Württemberg, Germany). The condensed products were analyzed by HPLC, using an Agilent Technologies 1260 Infinity instrument (Santa Clara, CA, USA) equipped with a DAD UV–Vis detector and an Agilent PORO shell 120 C-18 column. An external calibration method was used for the identification and quantification of reactants and products, using reference commercial samples.

4. Conclusions

The MFU production from FU was demonstrated to be strongly dependent on the nature and strength of the acidic sites coexisting on a basic support. The introduction of Fe as Lewis acid on MgO support led to the enhancement of the conversion of FU. The different methodologies employed to synthesize the catalysts and the different Fe/Mg ratios allowed to understand how the acidity is involved, not only in the FU activation, but also in its selective conversion to MFU. In fact, even if the simple impregnation of Fe₂O₃ on MgO led to satisfactory selectivity and activity, best results were obtained by coprecipitation, since this methodology led to the formation of Fe-containing mixed phases. Indeed, the presence of such highly dispersed phases was fundamental to modulate the distribution of acidic sites, which, in turn, allowed us to reach the targeted product (MFU) in high selectivity. Spectroscopic studies helped to understand the different activation modes of both methanol and furfural, indicating a possible reaction pathway.

Supplementary Materials: The following are available online at <http://www.mdpi.com/2073-4344/9/11/895/s1>. Figure S1: Pyridine-FTIR spectra of Fe/Mg/O_1_1 obtained after evacuation at different temperatures: (a) room temperature; (b) 100 °C; (c) 200 °C; (d) 300 °C; and (e) 400 °C. Figure S2: Pyridine-FTIR spectra of Fe/Mg/O_1_2 obtained after evacuation at different temperatures: (a) room temperature; (b) 100 °C; (c) 200 °C; (d) 300 °C; and (e) 400 °C. Figure S3: Pyridine-FTIR spectra of FeO_x/MgO_1_10 obtained after evacuation at different temperatures: (a) room temperature; (b) 100 °C; (c) 200 °C; (d) 300 °C; and (e) 400 °C. Figure S4: Pyridine-FTIR spectra of FeO_x/MgO_1_2 obtained after evacuation at different temperatures: (a) room temperature; (b) 100 °C; (c) 200 °C; (d) 300 °C; and (e) 400 °C. Figure S5: Furfural adsorption and desorption over MgO sample from RT to 400 °C. Figure S6: Furfural adsorption/desorption over FeO_x/MgO_1_10 sample from RT to 400 °C. Figure S7: FTIR spectra of Furfuryl alcohol adsorption/desorption over MgO at different temperature. Figure S8: Furfuryl alcohol adsorption/desorption over FeO_x/MgO_1_10 within different temperature.

Author Contributions: L.G., F.C., E.A.Q., and S.A. designed the different experiments and supported the interpretation of catalytic and catalyst characterization; L.G., D.B., and Y.Z. synthesized the catalysts and carried out catalytic evaluation and characterization of materials (XRD, TPD, and BET); Y.Z. and M.R.-C. carried out FTIR studies; C.L. supported FTIR interpretation; C.L., C.T., E.Q., N.D., and S.A. were involved in the writing and editing the manuscript.

Funding: This work was funded by SINCHEM Joint Doctorate Programme–Erasmus Mundus Action (framework agreement No. 2013-0037; specific grant agreement No. 2015-1600/001-001-EMJD).

Conflicts of Interest: The authors declare no conflict of interest.

References

1. Dusselier, M.; Sels, B.F. Selective Catalysis for Cellulose Conversion to Lactic Acid and Other α -Hydroxy Acids. In *Selective Catalysis for Renewable Feedstocks and Chemicals*; Nicholas, K.M., Ed.; Springer International Publishing: Cham, Switzerland, 2014; pp. 85–125.
2. Lolli, A.; Zhang, Y.; Basile, F.; Cavani, F.; Albonetti, S. Beyond H₂: Exploiting H-Transfer Reaction as a Tool for the Catalytic Reduction of Biomass. In *Chemicals and Fuels from Bio-Based Building Blocks*; Wiley-VCH Verlag GmbH & Co. KGaA: Weinheim, Germany, 2016; pp. 349–378.
3. Gilkey, M.J.; Xu, B. Heterogeneous Catalytic Transfer Hydrogenation as an Effective Pathway in Biomass Upgrading. *ACS Catal.* **2016**, *6*, 1420–1436. [[CrossRef](#)]
4. Scholz, D.; Aellig, C.; Hermans, I. Catalytic Transfer Hydrogenation/Hydrogenolysis for Reductive Upgrading of Furfural and 5-(Hydroxymethyl)furfural. *ChemSusChem* **2014**, *7*, 268–275. [[CrossRef](#)] [[PubMed](#)]
5. Sulmonetti, T.P.; Pang, S.H.; Claire, M.T.; Lee, S.; Cullen, D.A.; Agrawal, P.K.; Jones, C.W. Vapor phase hydrogenation of furfural over nickel mixed metal oxide catalysts derived from layered double hydroxides. *Appl. Catal. A Gen.* **2016**, *517*, 187–195. [[CrossRef](#)]
6. Manikandan, M.; Venugopal, A.K.; Nagpure, A.S.; Chilukuri, S.; Raja, T. Promotional effect of Fe on the performance of supported Cu catalyst for ambient pressure hydrogenation of furfural. *RSC Adv.* **2016**, *6*, 3888–3898. [[CrossRef](#)]
7. Lee, J.; Burt, S.P.; Carrero, C.A.; Alba-Rubio, A.C.; Ro, I.; O'Neill, B.J.; Kim, H.J.; Jackson, D.H.K.; Kuech, T.F.; Hermans, I.; et al. Stabilizing cobalt catalysts for aqueous-phase reactions by strong metal-support interaction. *J. Catal.* **2015**, *330*, 19–27. [[CrossRef](#)]

8. Wang, C.; Xu, H.; Daniel, R.; Ghafourian, A.; Herreros, J.M.; Shuai, S.; Ma, X. Combustion characteristics and emissions of 2-methylfuran compared to 2,5-dimethylfuran, gasoline and ethanol in a DISI engine. *Fuel* **2013**, *103*, 200–211. [[CrossRef](#)]
9. Xu, Y.; Qiu, S.; Long, J.; Wang, C.; Chang, J.; Tan, J.; Liu, Q.; Ma, L.; Wang, T.; Zhang, Q. In situ hydrogenation of furfural with additives over a RANEY Ni catalyst. *Rsc Adv.* **2015**, *5*, 91190–91195. [[CrossRef](#)]
10. Villaverde, M.M.; Garetto, T.F.; Marchi, A.J. Liquid-phase transfer hydrogenation of furfural to furfuryl alcohol on Cu–Mg–Al catalysts. *Catal. Commun.* **2015**, *58*, 6–10. [[CrossRef](#)]
11. Gong, L.-H.; Cai, Y.-Y.; Li, X.-H.; Zhang, Y.-N.; Su, J.; Chen, J.-S. Room-temperature transfer hydrogenation and fast separation of unsaturated compounds over heterogeneous catalysts in an aqueous solution of formic acid. *Green Chem.* **2014**, *16*, 3746–3751. [[CrossRef](#)]
12. Panagiotopoulou, P.; Martin, N.; Vlachos, D.G. Effect of hydrogen donor on liquid phase catalytic transfer hydrogenation of furfural over a Ru/RuO₂/C catalyst. *J. Mol. Catal. A: Chem.* **2014**, *392*, 223–228. [[CrossRef](#)]
13. Pasini, T.; Lolli, A.; Albonetti, S.; Cavani, F.; Mella, M. Methanol as a clean and efficient H-transfer reactant for carbonyl reduction: Scope, limitations, and reaction mechanism. *J. Catal.* **2014**, *317*, 206–219. [[CrossRef](#)]
14. Mironenko, A.V.; Vlachos, D.G. Conjugation-Driven “Reverse Mars–van Krevelen”-Type Radical Mechanism for Low-Temperature C–O Bond Activation. *J. Am. Chem. Soc.* **2016**, *138*, 8104–8113. [[CrossRef](#)] [[PubMed](#)]
15. Panagiotopoulou, P.; Vlachos, D.G. Liquid phase catalytic transfer hydrogenation of furfural over a Ru/C catalyst. *Appl. Catal. A: Gen.* **2014**, *480*, 17–24. [[CrossRef](#)]
16. Gilkey, M.J.; Panagiotopoulou, P.; Mironenko, A.V.; Jenness, G.R.; Vlachos, D.G.; Xu, B. Mechanistic Insights into Metal Lewis Acid-Mediated Catalytic Transfer Hydrogenation of Furfural to 2-Methylfuran. *Acs Catal.* **2015**, *5*, 3988–3994. [[CrossRef](#)]
17. Sitthisa, S.; Sooknoi, T.; Ma, Y.; Balbuena, P.B.; Resasco, D.E. Kinetics and mechanism of hydrogenation of furfural on Cu/SiO₂ catalysts. *J. Catal.* **2011**, *277*, 1–13. [[CrossRef](#)]
18. Sitthisa, S.; Resasco, D.E. Hydrodeoxygenation of Furfural Over Supported Metal Catalysts: A Comparative Study of Cu, Pd and Ni. *Catal. Lett.* **2011**, *141*, 784–791. [[CrossRef](#)]
19. Sitthisa, S.; Pham, T.; Prasomsri, T.; Sooknoi, T.; Mallinson, R.G.; Resasco, D.E. Conversion of furfural and 2-methylpentanal on Pd/SiO₂ and Pd–Cu/SiO₂ catalysts. *J. Catal.* **2011**, *280*, 17–27. [[CrossRef](#)]
20. Sitthisa, S.; An, W.; Resasco, D.E. Selective conversion of furfural to methylfuran over silica-supported NiFe bimetallic catalysts. *J. Catal.* **2011**, *284*, 90–101. [[CrossRef](#)]
21. Sheng, H.; Lobo, R.F. Iron-Promotion of Silica-Supported Copper Catalysts for Furfural Hydrodeoxygenation. *ChemCatChem* **2016**, *8*, 3402–3408. [[CrossRef](#)]
22. Grazia, L.; Lolli, A.; Folco, F.; Zhang, Y.; Albonetti, S.; Cavani, F. Gas-phase cascade upgrading of furfural to 2-methylfuran using methanol as a H-transfer reactant and MgO based catalysts. *Catal. Sci. Technol.* **2016**, *6*, 4418–4427. [[CrossRef](#)]
23. Crocella, V.; Cerrato, G.; Magnacca, G.; Morterra, C.; Cavani, F.; Maselli, L.; Passeri, S. Gas-phase phenol methylation over Mg/Me/O (Me = Al, Cr, Fe) catalysts: mechanistic implications due to different acid-base and dehydrogenating properties. *Dalton Trans.* **2010**, *39*, 8527–8537. [[CrossRef](#)] [[PubMed](#)]
24. Valente, J.S.; Figueras, F.; Gravelle, M.; Kumbhar, P.; Lopez, J.; Besse, J.P. Basic Properties of the Mixed Oxides Obtained by Thermal Decomposition of Hydrotalcites Containing Different Metallic Compositions. *J. Catal.* **2000**, *189*, 370–381. [[CrossRef](#)]
25. Sato, T.; Wakabayashi, T.; Shimada, M. Adsorption of various anions by magnesium aluminum oxide of (Mg_{0.7}Al_{0.3}O_{1.15}). *Ind. Eng. Chem. Prod. Res. Dev.* **1986**, *25*, 89–92. [[CrossRef](#)]
26. Tichit, D.; Lhouty, M.H.; Guida, A.; Chiche, B.H.; Figueras, F.; Auroux, A.; Bartolini, D.; Garrone, E. Textural Properties and Catalytic Activity of Hydrotalcites. *J. Catal.* **1995**, *151*, 50–59. [[CrossRef](#)]
27. Zhang, Y.; Wang, J.; Ren, J.; Liu, X.; Li, X.; Xia, Y.; Lu, G.; Wang, Y. Mesoporous niobium phosphate: an excellent solid acid for the dehydration of fructose to 5-hydroxymethylfurfural in water. *Catal. Sci. Technol.* **2012**, *2*, 2485–2491. [[CrossRef](#)]
28. Wang, F.; Ta, N.; Shen, W. MgO nanosheets, nanodisks, and nanofibers for the Meerwein–Ponndorf–Verley reaction. *Appl. Catal. A Gen.* **2014**, *475*, 76–81. [[CrossRef](#)]
29. Ballarini, N.; Cavani, F.; Maselli, L.; Montaletti, A.; Passeri, S.; Scagliarini, D.; Flego, C.; Perego, C. The transformations involving methanol in the acid- and base-catalyzed gas-phase methylation of phenol. *J. Catal.* **2007**, *251*, 423–436. [[CrossRef](#)]

30. Shao, Y.; Xia, Q.; Liu, X.; Lu, G.; Wang, Y. Pd/Nb₂O₅/SiO₂ Catalyst for the Direct Hydrodeoxygenation of Biomass-Related Compounds to Liquid Alkanes under Mild Conditions. *ChemSusChem* **2015**, *8*, 1761–1767. [CrossRef]
31. Hong, D.-Y.; Miller, S.J.; Agrawal, P.K.; Jones, C.W. Hydrodeoxygenation and coupling of aqueous phenolics over bifunctional zeolite-supported metal catalysts. *Chem. Commun.* **2010**, *46*, 1038–1040. [CrossRef]
32. Di Cosimo, J.I.; Díez, V.K.; Xu, M.; Iglesia, E.; Apesteguía, C.R. Structure and Surface and Catalytic Properties of Mg-Al Basic Oxides. *J. Catal.* **1998**, *178*, 499–510. [CrossRef]
33. Routray, K.; Zhou, W.; Kiely, C.J.; Wachs, I.E. Catalysis Science of Methanol Oxidation over Iron Vanadate Catalysts: Nature of the Catalytic Active Sites. *ACS Catal.* **2011**, *1*, 54–66. [CrossRef]
34. Badri, A.; Binet, C.; Lavalley, J.-C. Use of methanol as an IR molecular probe to study the surface of polycrystalline ceria. *J. Chem. Soc. Faraday Trans.* **1997**, *93*, 1159–1168. [CrossRef]
35. Tabanelli, T.; Passeri, S.; Guidetti, S.; Cavani, F.; Lucarelli, C.; Cargnoni, F.; Mella, M. A cascade mechanism for a simple reaction: The gas-phase methylation of phenol with methanol. *J. Catal.* **2019**, *370*, 447–460. [CrossRef]
36. Tabanelli, T.; Cocchi, S.; Gumina, B.; Izzo, L.; Mella, M.; Passeri, S.; Cavani, F.; Lucarelli, C.; Schütz, J.; Bonrath, W.; et al. Mg/Ga mixed-oxide catalysts for phenol methylation: Outstanding performance in 2,4,6-trimethylphenol synthesis with co-feeding of water. *Appl. Catal. A Gen.* **2018**, *552*, 86–97. [CrossRef]
37. Lucarelli, C.; Galli, S.; Maspero, A.; Cimino, A.; Bandinelli, C.; Lolli, A.; Velasquez Ochoa, J.; Vaccari, A.; Cavani, F.; Albonetti, S. Adsorbent–Adsorbate Interactions in the Oxidation of HMF Catalyzed by Ni-Based MOFs: A DRIFT and FT-IR Insight. *J. Phys. Chem. C* **2016**, *120*, 15310–15321. [CrossRef]
38. Chandramohan, P.; Srinivasan, M.P.; Velmurugan, S.; Narasimhan, S.V. Cation distribution and particle size effect on Raman spectrum of CoFe₂O₄. *J. Solid State Chem.* **2011**, *184*, 89–96. [CrossRef]
39. Nowicka, E.; Hofmann, J.P.; Parker, S.F.; Sankar, M.; Lari, G.M.; Kondrat, S.A.; Knight, D.W.; Bethell, D.; Weckhuysen, B.M.; Hutchings, G.J. In situ spectroscopic investigation of oxidative dehydrogenation and disproportionation of benzyl alcohol. *Phys. Chem. Chem. Phys.* **2013**, *15*, 12147–12155. [CrossRef]
40. Villa, A.; Ferri, D.; Campisi, S.; Chan-Thaw, C.E.; Lu, Y.; Kröcher, O.; Prati, L. Operando Attenuated Total Reflectance FTIR Spectroscopy: Studies on the Different Selectivity Observed in Benzyl Alcohol Oxidation. *ChemCatChem* **2015**, *7*, 2534–2541. [CrossRef]
41. Shekhar, R.; Barteau, M.A.; Plank, R.V.; Vohs, J.M. Adsorption and Reaction of Aldehydes on Pd Surfaces. *J. Phys. Chem. B* **1997**, *101*, 7939–7951. [CrossRef]
42. Davis, J.L.; Barteau, M.A. Spectroscopic identification of alkoxide, aldehyde, and acyl intermediates in alcohol decomposition on Pd(111). *Surf. Sci.* **1990**, *235*, 235–248. [CrossRef]
43. Socrates, G. *Infrared and Raman Characteristic Group Frequencies: Tables and Charts*; John Wiley & Sons: Hoboken, NJ, USA, 2004.
44. Dimas-Rivera, G.L.; De la Rosa, J.R.; Lucio-Ortiz, C.J.; De los Reyes Heredia, J.A.; González, V.G.; Hernández, T. Desorption of Furfural from Bimetallic Pt-Fe Oxides/Alumina Catalysts. *Materials* **2014**, *7*, 527–541. [CrossRef] [PubMed]
45. Available online: https://sdbs.db.aist.go.jp/sdbs/cgi-bin/direct_frame_top.cgi (accessed on 27 October 2019).
46. Rogojevov, M.; Keresztury, G.; Jordanov, B. Vibrational spectra of partially oriented molecules having two conformers in nematic and isotropic solutions: furfural and 2-chlorobenzaldehyde. *Spectrochim. Acta Part A Mol. Biomol. Spectrosc.* **2005**, *61*, 1661–1670. [CrossRef] [PubMed]
47. Shen, J.; Wang, M.; Wu, Y.-n.; Li, F. Preparation of mesoporous carbon nanofibers from the electrospun poly(furfuryl alcohol)/poly(vinyl acetate)/silica composites. *RSC Adv.* **2014**, *4*, 21089–21092. [CrossRef]
48. Cesari, C.; Mazzoni, R.; Matteucci, E.; Baschieri, A.; Sambri, L.; Mella, M.; Tagliabue, A.; Basile, F.L.; Lucarelli, C. Hydrogen Transfer Activation via Stabilization of Coordinatively Vacant Sites: Tuning Long-Range π -System Electronic Interaction between Ru(0) and NHC Pendants. *Organometallics* **2019**, *38*, 1041–1051. [CrossRef]
49. Albonetti, S.; Boanini, E.; Jiménez-Morales, I.; Lucarelli, C.; Mella, M.; Molinari, C.; Vaccari, A. Novel thiotolerant catalysts for the on-board partial dehydrogenation of jet fuels. *RSC Adv.* **2016**, *6*, 48962–48972. [CrossRef]

50. Lucarelli, C.; Giugni, A.; Moroso, G.; Vaccari, A. FT-IR Investigation of Methoxy Substituted Benzenes Adsorbed on Solid Acid Catalysts. *J. Phys. Chem. C* **2012**, *116*, 21308–21317. [[CrossRef](#)]
51. Grazia, L.; Bonincontro, D.; Lolli, A.; Tabanelli, T.; Lucarelli, C.; Albonetti, S.; Cavani, F. Exploiting H-transfer as a tool for the catalytic reduction of bio-based building blocks: the gas-phase production of 2-methylfurfural using a FeVO₄ catalyst. *Green Chem.* **2017**, *19*, 4412–4422. [[CrossRef](#)]



© 2019 by the authors. Licensee MDPI, Basel, Switzerland. This article is an open access article distributed under the terms and conditions of the Creative Commons Attribution (CC BY) license (<http://creativecommons.org/licenses/by/4.0/>).